Compact 1 × *N* power splitters with arbitrary power ratio for integrated multimode photonics

OPEN ACCESS
IOP Publishing
Journal of Optics
J. Opt. **23** (2021) 095802 (9pp)
https://doi.org/10.1088/2040-8986/ac1830

Compact 1 × *N* power splitters with arbitrary power ratio for integrated multimode photonics

Yohann Franz and Massimiliano Guasoni*

Optoelectronics Research Centre, University of Southampton, Southampton, SO17 1BJ, United Kingdom

E-mail: m.guasoni@soton.ac.uk

Received 26 March 2021, revised 3 July 2021
Accepted for publication 27 July 2021
Published 31 August 2021

Abstract

We introduce a 1 × *N* integrated power splitter for the multimode photonics platform. The device converts an input laser beam into a higher-order mode beam, which afterwards is split. The core of this setup is represented by a non-uniform array of *N* waveguides that allows achieving arbitrary power splitting. The system exhibits high modal purity and is tested against wavelength variations and fabrication errors. The possibility to include a multi-input port configuration, leading to various power ratios via a single device, provides further flexibility. Our analysis is validated by finite-element-method simulations. At the best of our knowledge, this represents the first design of a device for arbitrary 1 × *N* power splitting of higher-order modes.

Keywords: optical power splitter, multimode photonics, integrated photonics, waveguide arrays

(Some figures may appear in colour only in the online journal)

1. Introduction

Optical beam splitters are key building blocks of photonic integrated circuits (PICs). Besides the obvious ability to split and deliver the optical power in different points of a PIC, they are at the core of several devices ranging from Mach–Zehnder interferometers [1] up to optical filters [2] and equalizers [3]. The design of compact splitters is therefore functional to the development of high-density, small and low-power consuming PIC technology.

Traditionally, on-chip 1 × *N* splitters are realized through either cascade Y-junctions [4–6] or multimode interference (MMI) structures [7–11]. The first benefit from a low sensitivity to wavelength variation, leading to flat spectral response. However, cascaded systems typically suffer a large footprint. Moreover, arbitrary splitting is achieved at the expense of complex asymmetric structures even in the most simple case of a 1 × 2 splitter [12]. MMI devices exhibit a more compact size and good fabrication tolerance. Nevertheless, arbitrary power splitting requires either the support of external thermo-optical or electro-optical modulators or the design of complex configurations (e.g. butterfly geometry or cascade systems), which are practically limited to the case of 1 × 2 or 1 × 3 splitters and make the device less robust against fabrication imperfections [11, 13–15].

In this paper, we propose an alternative scheme for on-chip power splitting, which is based on an array of waveguides having non-uniform separation (non-uniform array). A beam injected at the array input is split due to the coupling among the waveguides. The splitting dynamics depends essentially on the distance between adjacent waveguides and can therefore be controlled by proper array design so as to achieve an arbitrary power splitting ratio without resorting to complex geometries.

In addition, the proposed system can be designed so as to achieve 1 × *N* splitting of a given higher-order mode beam of choice. In the last decade, multimode photonics has attracted massive interest as it offers the tantalised prospect to extend

* Author to whom any correspondence should be addressed.

the capabilities of the single-mode counterpart [16–21]. The implementation of $1 \times N$ splitters of higher-order mode beams is therefore a key operation as in the single-mode platform. Since multimode photonics is a relatively young field of study, this is a quite recent topic. In 2019 [22], a few-mode 1×2 splitter has been proposed providing equal (non-arbitrary) splitting. In 2020 [23], a MMI-based $1 \times N$ equal splitter has been demonstrated working at 1.55 μm, and a T-junction based 1×2 splitter [24] has been proposed. At the best of our knowledge, our paper reports the first design of $1 \times N$ power splitters for multimode photonics providing arbitrary power ratio and spanning a bandwidth up to several tens of nanometers (in the C-band). As such, we believe it will stimulate the research into novel setups for the all-optical control of light in multimode systems.

This work is organised as follows. In section 2, we introduce the principle of operation and the governing equations that describe light propagation in the system under study. In sections 3 and 4, we discuss two examples of 1×5 power splitters, investigating the robustness against fabrication errors and wavelength variations. In section 5, we discuss the possibility to obtain arbitrary power splitting ratios as well as a multi-input port configuration that allows achieving different power ratios with the same device. Section 6 sums up the main results and conclusions. In the Appendix, we provide some analytical tools to evaluate the modal purity at the output ports of the array.

2. Principle of operation

The system under analysis consists of the three stages represented in figure 1.

Stage-1 is a directional coupler with asymmetric waveguides, which is used to generate a higher order mode. Therefore, this stage is not needed if the higher-order mode is generated externally or if we aim to split the fundamental modes quasi-TE00/TM00 (hereafter we omit the prefix quasi- for the sake of simplicity). The input waveguide of the coupler is excited by an external laser beam coupled to the TE00 (TM00) mode. By properly setting the width of the two waveguides, the TE00(TM00) mode of the input waveguide is phase-matched with one specific higher-order mode of the output waveguide [25]. This leads to an effective conversion from the TE00 (TM00) mode to the higher-order mode in the output waveguide. The output waveguide of the coupler is prolonged and becomes the input waveguide of stage-2.

Stage-2 is an array of N identical waveguides that represent the core of the proposed device. The coupling among the waveguides splits the beam in input from stage-1 into several replica. Hereafter, we indicate with W_n the waveguides of the array numbered from $n = 1$ to $n = N$ (see figure 1). Differently from standard uniform arrays, where the distance between each pair of adjacent waveguides is the same, here each pair of adjacent waveguides W_n and W_{n-1} is separated by a distinct distance $d_{n-1,n}$ (see figure 1). The system is therefore

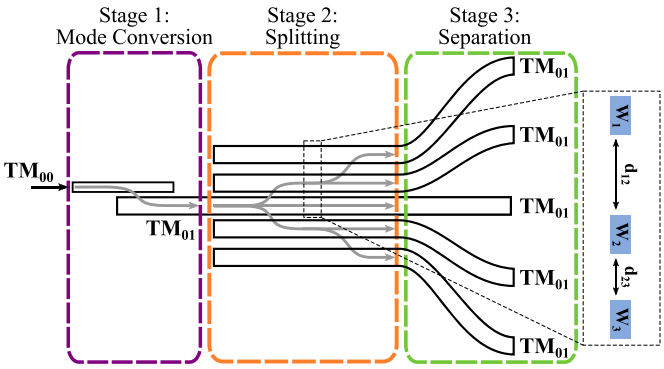

Figure 1. Schematic of the power splitter. The mode converter in stage-1 converts an external laser beam to a higher order mode beam (which is TM01 in this example). In stage-2, the beam is split among the different waveguides of the non-uniform array. An arbitrary splitting ratio is achieved by proper design of the array geometry (length and distances among the waveguides).The optional stage-3 allows increasing the separation between the beams at the system output. The inset on the right shows the notation used in this paper to indicate waveguides (W_1, W_2, W_3) and distances (d_{12}, d_{23}).

characterized by N degrees of freedoms, namely, the array length L and the $(N-1)$ distances between the different pairs of adjacent waveguides. This allows controlling the power of all the N replica at the array output. In other words, by properly setting the array length and the distances between the waveguides, we can impose an arbitrary output power distribution. This is not possible in a uniform array, where the uniform distance among adjacent waveguides reduces to two the degrees of freedom.

When the dynamics is dominated by the linear coupling among adjacent waveguides (nearest-neighbour approach), light propagation in the array is well described by the following system of ordinary differential equations [26]:

$$\begin{aligned}\partial_z A(n,z) = j\beta_n \cdot A(n,z) + jC_{n,n-1} \cdot A(n-1,z) \\ + jC_{n,n+1} \cdot A(n+1,z)\end{aligned} \tag{1}$$

where $A(n,z)$ and β_n are respectively the amplitude of the beam in waveguide W_n and its corresponding wave-vector, whereas $C_{n,n-1}$ ($C_{n,n+1}$) is the coupling coefficient between the waveguides W_n and W_{n-1} (W_n and W_{n+1}). Both the wave-vectors and the coupling coefficients refer to the spatial mode in input at the array from stage-1 (e.g. mode TM01 in figure 1). Note that for the first ($n = 1$) and the last ($n = N$) waveguide of the array coupling occurs only with one neighbour, therefore the corresponding equations reduce to $\partial_z A(1,z) = j\beta_1 A(1,z) + jC_{1,2} \cdot A(2,z)$ and $\partial_z A(N,z) = j\beta_N A(N,z) + jC_{N,N-1} \cdot A(N-1,z)$, respectively. The coupling coefficients are calculated as follows [27]:

$$C_{n,n-1} = C_{n-1,n} = \frac{1}{2}\left(\beta^{(ev)}_{n,n-1}(d) - \beta^{(od)}_{n,n-1}(d)\right) \tag{2}$$

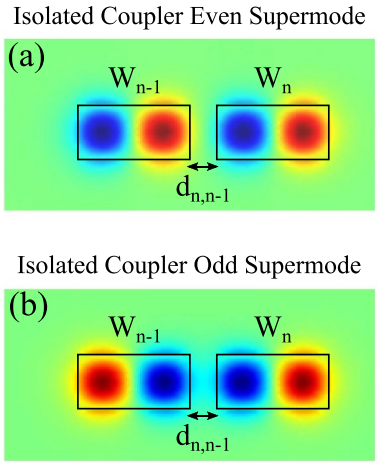

Figure 2. The coupling coefficient $C_{n-1,n}$ is computed from the supermodes of the isolated coupler formed by waveguides W_{n-1} and W_n. The supermodes under consideration are those related to the mode in input at the array. For example, if the mode in input at the array is TM01, as in figure 1, then the even and odd supermodes to consider are those respectively formed by the combination in-phase (panel (a)) and anti-phase (panel (b)) of the mode TM01 in waveguides W_{n-1} and W_n.

where $d \equiv d_{n,n-1}$, $\beta^{(ev)}_{n,n-1}(d)$ and $\beta^{(od)}_{n,n-1}(d)$ represent respectively the wave-vectors of the even and the odd supermodes of the isolated coupler formed by waveguides W_n and W_{n-1} separated by a distance d, as illustrated in figure 2. The formula in equation (2) provides an accurate estimation of the coupling length among adjacent waveguides even in the case of strong coupling (i.e. very close waveguides), which is critical to the design of compact arrays. This is confirmed by comparison with finite-element-method (FEM) simulations, as discussed in the next sections.

The system of differential equation (1) is completed with the boundary conditions that define the input and output amplitudes $A(n, z=0)$ and $A(n, z=L)$, respectively. In the system under analysis, only one waveguide $W_{n_{in}}$ of the array is fed in input (in figure 1 $W_{n_{in}} = W_3$ is the central waveguide), therefore the input condition reads $A(n_{in}, z=0) = A_0$, A_0 being the input amplitude; whereas $A(n, z=0) = 0$ for all the other waveguides W_n with $n \neq n_{in}$.The output condition is arbitrarily chosen based on the desired splitting ratio. For example, if we target an equal power splitting then we impose all the output amplitudes $A(n, z=L)$ to have the same magnitude, that is, $|A(1, z=L)| = |A(n, z=L)|\ \forall n$.

Given equation (1) along with the above-mentioned input and output boundary conditions, we can then recover the corresponding coupling coefficients and the array length. Once the coupling coefficients $C_{n,n-1}$ are found, we calculate the corresponding distances $d_{n,n-1}$ among the waveguides W_n and W_{n-1}.

The final result is that we determine the array geometry (distances between waveguides and length of the array) leading to the desired power splitting ratio at the array output.

The last stage of the system under analysis is stage-3. In this optional stage the separation among adjacent waveguides is increased as illustrated in figure 1, which could facilitate the independent manipulation of the beams at the system output.

3. Design of a TE00 1 × 5 equal power splitter

In this section, we design a power splitter based on the principles illustrated in the previous section. We focus on the simplest scenario where the mode in input at the array is the fundamental mode TE00, which does not require any mode conversion. Consequently, stage-1 is not present. We also ignore stage-3 at the moment and focus only on stage-2, which is the core of the system. A complete example including stages-1 and 3, as well as the use of a higher-order mode, is reported in section 4.

We focus here on a 1×5 splitter, however the design could be easily scaled up to a larger number N. The array is made of five identical 400×300 nm silicon waveguides embedded in silica, with the central waveguide W_3 excited by a TE00 beam at the input. The input boundary condition reads therefore: $A(3, z=0) = A_0, A(n, z=0) = 0$ for $n = \{1,2,4,5\}$. For the sake of simplicity, we consider here a symmetric geometry with respect to the central waveguide W_3, namely, with distances $d_{12} = d_{45}$ and $d_{23} = d_{34}$. Under this condition, the solution of equation (1) takes a relatively simple form, which is:

$$\begin{aligned} |A(1,z)| = |A(5,z)| &= \left| \frac{A_0 R}{p^2} - \frac{A_0 R}{p^2} \cos(C_{12} p z) \right| \\ |A(2,z)| = |A(4,z)| &= \left| \frac{A_0 R}{p} \sin(C_{12} p z) \right| \\ |A(3,z)| &= \left| \frac{A_0}{p^2} + \frac{2A_0 R^2}{p^2} \cos(C_{12} p z) \right| \end{aligned} \tag{3}$$

where $R = C_{23}/C_{12}$ and $p = (1+2R^2)^{1/2}$. From equation (3), we see that the evolution of the amplitudes $A(n,z)$ depends only on the product $C_{12}z$ and the ratio R. Therefore, the power distribution at the array output does not change if the array length is increased (decreased) by a given factor and the coupling coefficients are simultaneously decreased (increased) by the same factor. This rescaling property can be generalised to the case of an arbitrary number N of waveguides, and provides a useful degree of freedom when one wants to resize the array so as to increase or decrease the total length or the distance between the waveguides.

Let us now consider the case of equal splitting where all the five waveguides share the same amount of power at the output, namely $|A(n, z=L)|^2 = 0.2A_0^2\ \forall n$, where ${A_0}^2$ is the total input power at the array. Under this output boundary condition, two distinct solutions of equation (3) are found that read $R = 0.618$, $C_{12}L = |1.393 + 2\pi k/p|$ and $R = 1.618$, $C_{12}L = |0.953 + 2\pi k/p|$, with $k \in \mathbb{Z}$. Without loss of generality, we focus here on the case $R = 1.618$, $C_{12}L = 0.953$ and we fix the operation wavelength $\lambda = 1.55\ \mu$m.

Figure 3 displays the coupling coefficient computed from equation (2) (for mode TE00) at $\lambda = 1.55\ \mu$m and as a function of the distance between adjacent waveguides. Clearly,

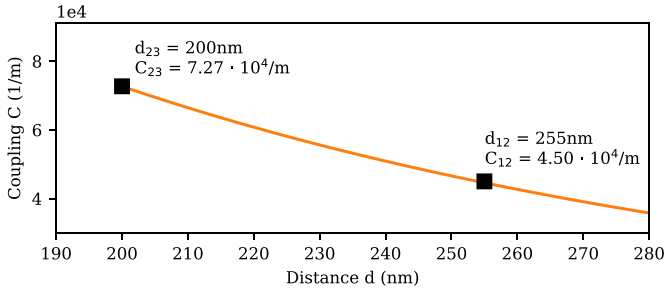

Figure 3. Coupling coefficient vs distance computed from equation (2) for the case of Si-waveguides in silica cladding. Waveguides size is 400 × 300 nm. The black squares highlight the value of the coupling coefficients C_{12} and C_{23} when the distance is set respectively to $d \equiv d_{12} = 255$ nm and $d \equiv d_{23} = 200$ nm. These coefficients satisfy the relation $R = C_{23}/C_{12} = 1.618$.

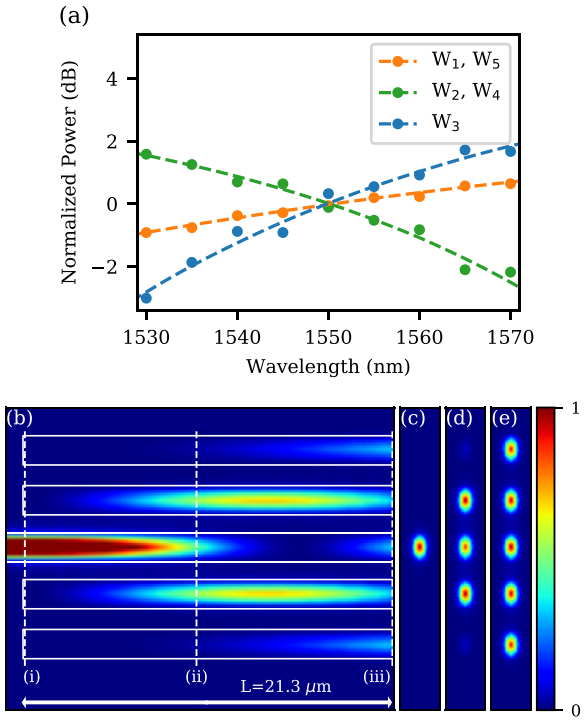

Figure 4. (a) Normalized power vs wavelength for waveguides $W_{1,2,3,4,5}$ at the output of the 1 × 5 array. Both analytical results (dashed lines) as per equation (3) and results from FEM simulations (circles) are reported. (b) FEM simulation of the array at $\lambda = 1.55$ μm illustrating the evolution of the normalized magnitude of the electric field. (c)–(e) Cross sections at positions (i), (ii) and (iii), respectively.

there are infinite pairs $\{d_{12}, d_{23}\}$ that satisfy the relation $R = C_{23}/C_{12} = 1.618$. However, in our case the aim is designing a compact array: with this in mind, we choose the relatively small distances $d_{12} = 255$ nm and $d_{23} = 200$ nm. As we can see from figure 3, the corresponding coupling coefficients are $C_{12} = 4.50 \times 10^4$ m^{-1} and $C_{23} = 7.27 \times 10^4$ m^{-1}. Finally, from the relation $C_{12}L = 0.953$, we find the array length, which is $L = 21.18$ μm. This concludes the array design: the distances d_{12}, d_{23} and the array length L have been identified that allow equal splitting at the array output.

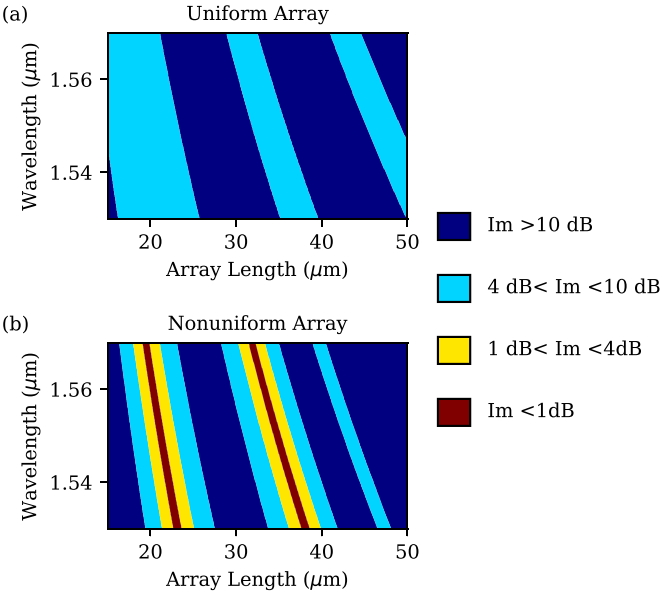

Figure 5. Illustration of power imbalance *Im* for the uniform (a) and non-uniform (b) 1 × 5 array. Different colours identify different levels of *Im*. In the case of the uniform array the power imbalance is remarkable (>4 dB) at each wavelength. On the contrary, in the case of the non-uniform array equal splitting (*Im* = 0 dB) can be achieved at any wavelength for a proper array length. Note that the line of equal splitting (not illustrated) lies within the red region, which identifies the points where *Im* < 1 dB.

It should be noted however that these parameters are strictly valid at the reference wavelength $\lambda = 1.55$ μm. In order to test the system bandwidth, we run numerical simulations for input wavelengths in the range 1.50–1.60 μm. In first instance, we use the formulas in equation (3) to calculate the power $|A(n, z = L)|^2$ at the output of waveguide W_n. For each wavelength under test, the coupling coefficients C_{12} and C_{23} are calculated from equation (2) by taking into account for the material dispersion of silicon [28] and silica [29]. In figure 4(a), we report the output power normalized to $0.2A_0^2$ (so that 0 dB indicates equal splitting). As expected, almost equal splitting is found at 1.55 μm. In addition, the output power in each waveguide exhibits ±0.5 dB uniformity in the band 1.547–1.557 μm.

In order to confirm the validity of the aforementioned results and of the model described by equations (1) and (3), FEM simulations of the array have been performed (figure 4(b)). In these simulations, the input beam at the array is the fundamental mode TE00 of the central waveguide. At the output of the array, the power coupled to the mode TE00 in the waveguide W_n is computed through modal decomposition as detailed in the Appendix. As reported in figure 4(a), the results of the FEM simulations match well the analytical predictions of equation (3).

It is worth noting that the non-uniformity of the array is the key-feature leading to the desired equal splitting in this example and, more in general, to any arbitrary power splitting. This is actually not achievable through standard uniform arrays. Figure 5 compares the power imbalance *Im* between the maximum and minimum powers at the output of a 1 × 5 uniform array ($d_{12} = d_{23} = 200$ nm) and of the

non-uniform array under test ($d_{12} = 255$ nm, $d_{23} = 200$ nm), namely, $Im = \max_n\{|A(n, z = L)|^2\}/\min_m\{|A(m, z = L)|^2\}$. We see that the uniform array does not allow to achieve equal power splitting, whereas in the case of the non-uniform array equal splitting ($Im = 0$ dB) can be achieved at any wavelength for a proper array length.

4. Design of a TM01 1 × 5 equal power splitter

In this section, we illustrate a system that performs mode conversion in stage-1, then splitting in stage-2 and finally waveguide separation in stage-3.

The mode converter of stage-1 is displayed in figure 6. In this example, an external laser beam is coupled to the TM00 mode at the input waveguide of the mode converter (figure 6(b)), which is then converted to a TM01 beam in the output waveguide (figure 6(d)). The conversion is maximized under the phase-matching condition $n_{00}^{(\mathrm{in})} = n_{01}^{(\mathrm{out})}$, where $n_{00}^{(\mathrm{in})}$ and $n_{01}^{(\mathrm{out})}$ are respectively the effective index of mode TM00 in the input waveguide and of mode TM01 in the output waveguide [25]. From figure 6(a), we observe that this condition is achieved when the widths of the input and output waveguides are 275 nm and 700 nm, respectively (at $\lambda = 1.55$ μm and for a thickness of 500 nm, which allows strong confinement of the TM01 mode). The distance between the input and output waveguide is not a critical parameter, but rather defines the coupling length for which effective TM00 to TM01 conversion occurs. The FEM simulation displayed in figure 6(c) shows that when the distance is 90 nm then the coupling length is ~ 4.05 μm. Moreover, the mode converter has large bandwidth, since large conversion >93% is obtained in the whole spectral range from 1.50 to 1.575 μm.

The output waveguide of the mode converter is prolonged and becomes the input waveguide for the array in stage-2. Here, we still focus on a 1×5 array symmetric with respect to the central waveguide W_3, so that the analytical solutions in equation (3) hold true. Waveguide W_3 plays the role of input waveguide for the array (as in figure 1). In this example the array waveguides have the same size of the output waveguide of the mode converter, which is 700×500 nm. This allows minimising the reflection losses at the interface between stage-1 and stage-2. Note however that a taper could be used to accommodate a different size.

The design of the array follows the same steps outlined in the previous section. We first compute the coupling coefficient versus the distance among adjacent waveguides from equation (2), and we find therefore two distances d_{12} and d_{23} such that the corresponding ratio $R = C_{23}/C_{12} = 1.618$. Finally, the optimal array length $L = 0.953/C_{12}$ is found. In this example, the parameters turn out to be $d_{12} = 251$ nm, $d_{23} = 200$ nm and $L = 16.39$ μm.

When one wants to increase the separation among the output beams of the array, stage-3 is implemented. It is worth noting that reflection and radiation losses (see Appendix) turn out to be negligible thanks to the large radius of curvature in stage-3 and the minimisation of discontinuities along the propagation direction. As a general rule, for a given waveguide geometry, spatial mode and wavelength, it is always possible to find a radius of curvature beyond which radiation losses become negligible. In the example under analysis, the FEM simulations show that radiation losses are <–20 dB for all the modes when the radius is 8 μm, which is used in external waveguides $W_{1,5}$ (whereas it is 12 μm for $W_{2,4}$). Absorption losses, which are of the order of 1 dB cm^{-1} in silicon, are negligible as well due to the short propagation distance. Note also that at the entry of stage-3 the waveguides are still strongly coupled. The coupling then decreases as long as the separation among the waveguides increases, until the waveguides are finally fully decoupled. Therefore, in order to account for the initial coupling in stage-3, the optimal length of stage-2 previously calculated ($L = 16.39$ μm) is reduced to $L = 14.35$ μm. Our FEM simulations are summarised in figure 7. Figures 7(e) and (f) display the output power normalized to $0.2A_0{}^2$ and coupled to modes TM00 and TM01. High modal purity is found (see Appendix), with >15 dB extinction ratio between the TM01 and the TM00 mode at each wavelength. Even larger extinction ratios (>30 dB) are found between the TM01 mode and the other guided modes. We can see in figure 7(e) that all the waveguides exhibit almost equal power splitting with ±0.5 dB uniformity over a bandwidth of ∼12 nm centred at 1.55 μm.

We point out that both the actual width of the waveguides and their mutual distances could deviate from the designed values due to fabrication errors. This may impact the ability to achieve the desired power splitting ratio at the

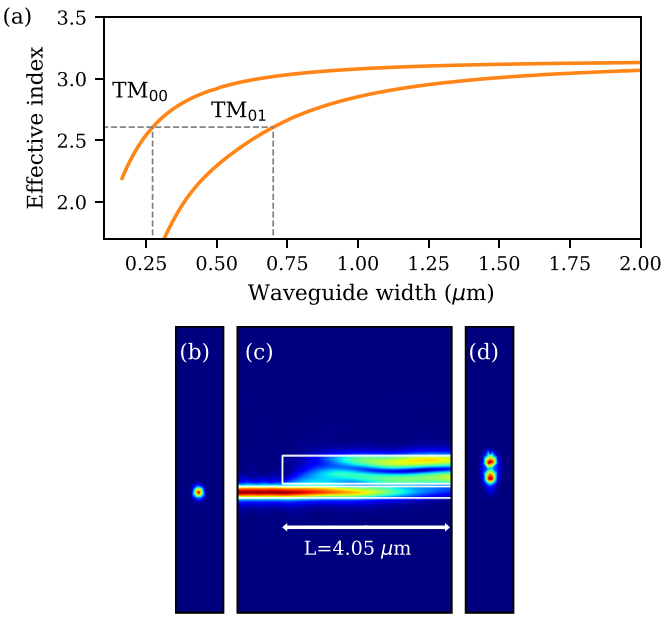

Figure 6. (a) Effective indexes of the TM00 and TM01 modes as a function of the waveguide width at $\lambda = 1.55$ μm (fixed thickness = 500 nm). The two effective indexes are equal when the widths are respectively 275 nm and 700 nm (see dashed lines). (b)–(d) FEM simulation of the mode converter (stage-1) at $\lambda = 1.55$ μm. The input waveguide is excited with a TM00 beam (see cross section in panel (b)), which is then converted into a TM01 beam in the output waveguide (see cross-section in panel (d)).

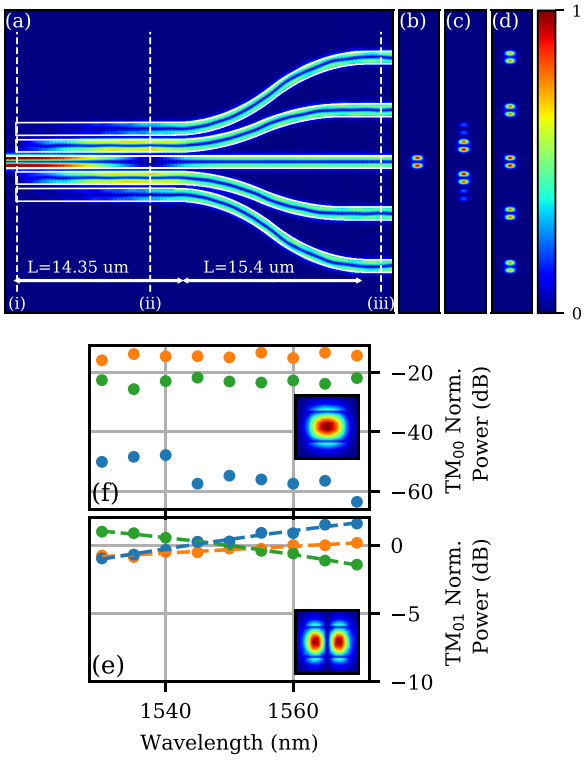

Figure 7. (a) FEM simulation of the TM01 1×5 splitter (stage-2 and stage-3) at $\lambda = 1.55$ μm, illustrating the evolution of the normalized magnitude of the electric field. (b)–(d) Cross sections at positions (i), (ii) and (iii), respectively. (e)–(f) Normalized output power coupled to modes TM00 and TM01 in waveguides $W_{1,5}$ (orange), $W_{2,4}$ (green), W_3 (blue).

system output. Indeed, on the one hand a variation of the relative size among waveguides induces a phase-mismatch and consequently reduces the maximum transfer of energy from one waveguide to another; and on the other hand, a random variation of the distance between two adjacent waveguides induces a random variation of their coupling length. We have therefore tested the system performance by adding a random deviation of ± 7.5 nm to all the waveguides widths and their mutual distances. This deviation is compatible with fabrication errors in standard lithography [30, 31]. When introducing this random deviation, the array symmetry with respect to the central waveguide is lost and we cannot therefore rely on equation (3). One must solve numerically equation (1), where contrary to the previous case the propagation constants β_n are generally different each other, and similarly all the coupling coefficients $C_{n,n-1}$ and $C_{n,n+1}$ must be computed by taking into account the specific size and distance for each couple of waveguides. The main outcome of this analysis is that the system is robust against random deviations. Indeed, the 12 nm bandwidth is preserved, the only difference being that the central wavelength of the bandwidth, rather than being fixed at 1.55 μm, is randomly distributed in the range 1.547–1.553 μm. In other words, one should accept a deviation of ± 3 nm of the central wavelength. It should be noted that the impact of fabrication errors can be mitigated by increasing the waveguides width, which reduces the relative error induced by the ± 7.5 nm random deviation.

More in general, we believe that by proper optimizing the array length and the coupling coefficients (also exploiting the rescaling property discussed in section 3), one may be able to increase both the device robustness and bandwidth. This is however a complex topic that would deserve a separate investigation.

5. System flexibility: arbitrary power splitting and multi-input systems

The design principles illustrated in the previous sections can be exploited to achieve an arbitrary power splitting ratio at the output, which represents a distinctive feature of the system under analysis. As anticipated in section 1, differently from MMI or Y-junctions cascaded structures, here the system complexity does not increase when targeting non-equal splitting. The design of stage-1 and stage-3 remains unaltered, whereas stage-2 is still an array of straight waveguides whose mutual distances are properly set so as to achieve the targeted splitting ratio.

Figure 8 illustrates two examples that refer to a TM01 power splitter. In both cases stage-1 is the same as in the previous section, allowing conversion from TM00 to TM01, and the waveguides in stage-2 are 700×500 nm. However, in the first case displayed in figure 8(a), rather than targeting equal splitting (20%) at all the output waveguides, we target instead equal splitting in four out five waveguides, which are $W_{1,2,4,5}$ with 24.5% power ratio. This is equivalent to a 1×4 equal splitter with a small amount of residual power (2%) in the central waveguide W_3 to be used for monitor/feedback purposes. We can still use the analytical formulas in equation (3) with input boundary condition $|A(3, z = 0)|^2 = A_0^2$, $A(n, z = 0) = 0$ for $n = \{1, 2, 4, 5\}$). However, in this case the output boundary condition reads $|A(n, z = L)|^2 = A_0^2 \cdot 0.245$ ($n = \{1, 2, 4, 5\}$) and $|A(3, z = L)|^2 = A_0^2 \cdot 0.02$. One solution of equation (3) under these boundary conditions is given by $R = C_{23}/C_{12} = 1.387$ and $L = 1.04/C_{12}$. We choose $C_{12} = 6.78 \times 10^4$ m^{-1} and $C_{23} = 9.41 \times 10$ m^{-1}, to which it finally corresponds $d_{12} = 235$ nm, $d_{23} = 200$ nm and L = 15.33 μm. Figure 8(a) shows the normalized power at the output of the corresponding array. We observe that the targeted 1×4 equal splitting in the external waveguides $W_{1,2,4,5}$ is achieved with uniformity of $\pm$ 0.4 dB across the C-band 1.53–1.56 μm.

Figure 8(b) displays a different example where the targeted splitting ratios for the waveguides from W_1 to W_5 are respectively 30%, 15%, 10%, 15% and 30%. Following the same steps illustrated in the previous examples, we find that this splitting ratio can be achieved by setting $d_{12} = 200$ nm, $d_{23} = 250$ nm and L = 17.27 μm.

As a further evidence of the flexibility offered by our system, we point out that different power splitting ratios can be achieved depending on the input waveguide used to

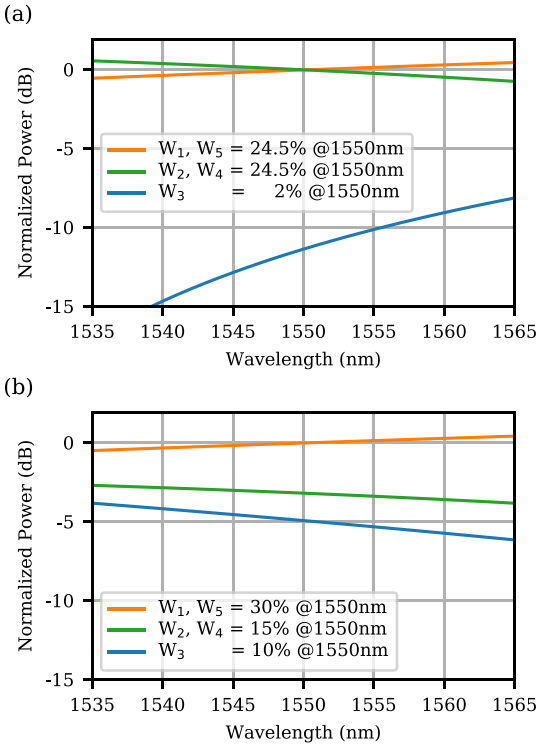

Figure 8. Normalized power vs wavelength for two different TM01 splitters. (a) The array has $d_{12} = d_{45} = 235$ nm, $d_{23} = d_{34} = 200$ nm and $L = 15.33$ μm. Equal splitting (24.5%) with uniformity ± 0.5 dB is reached across the C-band in waveguides $W_{1,2,4,5}$, with small residual power in the central waveguide (2% at $\lambda = 1.55$ μm). (b) The array has $d_{12} = d_{45} = 200$ nm, $d_{23} = d_{34} = 250$ nm and $L = 17.27$ μm. Unequal splitting is achieved, being 30% in waveguides $W_{1,5}$ (± 0.5 dB uniformity across the C-band), 15% in waveguides $W_{2,4}$ (± 0.5 dB uniformity) and 10% in waveguides W_3 (± 1 dB uniformity).

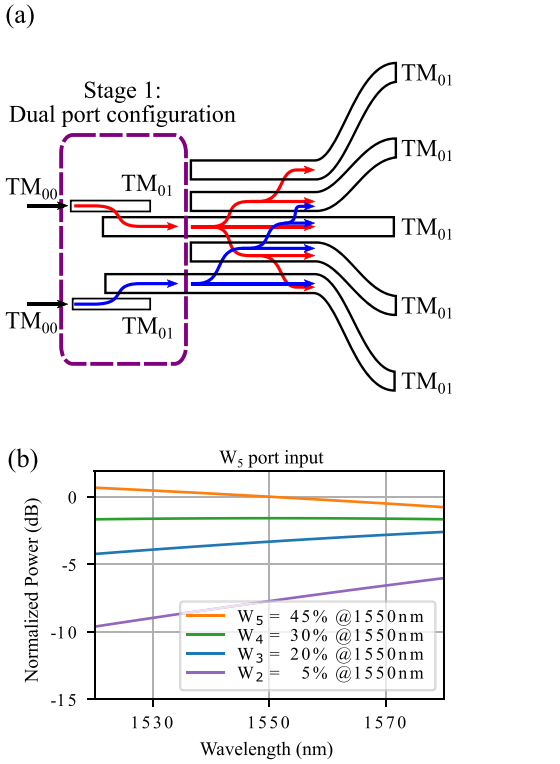

Figure 9. (a) Multi-input system. Two distinct and uncoupled mode-converters in stage-1 allow injecting the TM01 mode on either waveguide W_3 (red arrows) or W_5 (blue arrows) of the array, leading to different power ratios. (b) Normalized output power (coupled to mode TM01) when the input waveguide is W_5. Note: the case of W_3 input waveguide is illustrated in figure 7.

feed the array. This idea of multi-input port configuration is illustrated in figure 9, where two independent mode converters are present in stage-1 so that the input waveguide to stage-2 can be either W_3 or W_5. Let us consider for example the array designed in section 4, with $d_{12} = 251$ nm, $d_{23} = 200$ nm and L = 14.35 μm. We have already seen in section 4 that when the input waveguide to stage-2 is W_3, then we obtain equal splitting with ± 0.5 dB uniformity over a bandwidth of 12 nm (see figure 7). However, when feeding the array from waveguide W_5 ($A(5, z = 0) = A_0$, $A(n, z = 0) = 0$ for $n = \{1, 2, 3, 4\}$), we obtain unequal power splitting ratio of 45%, 30%, 20% respectively in waveguides W_5, W_4, W_3 with $< \pm 0.5$ dB uniformity across the C-band, whereas 5% power ratio in W_2 with ± 1 dB uniformity.

We stress however that it is not possible, in general, to design the array in such a way to achieve two arbitrary power ratios for two different input waveguides. This would indeed require $2N$ degrees of freedom, whereas only N are available as previously discussed. In other words, we can design an array geometry that provides an arbitrary splitting ratio for a given input waveguide; however, this geometry fixes the splitting ratio that is obtained when entering from a different waveguide.

6. Conclusion

In this paper, we have introduced a new setup for the implementation of a $1 \times N$ integrated power splitter. The system consists of a mode converter that allows conversion of the input laser beam into a higher order spatial mode of choice, which is followed by an array of coupled waveguides. An optional stage can be added to increase the separation between the output waveguides. The non-uniformity of the array turns out to be the key to achieve arbitrary power splitting at the output, which is generally not possible in standard uniform arrays. The strong coupling among the array waveguides leads to efficient splitting within a relatively short propagation distance, which makes the total array footprint of the order of 10 μm^2 per waveguide.

The propagation of light in the array is well described by the coupled equations (1). These equations, along with the boundary conditions, allow a straightforward inverse design of the array geometry.

Finite-element-method simulations validate the model and demonstrate that high-modal purity is achieved at the system output. A few examples of 1×5 splitters robust against fabrication errors have been provided, exhibiting a bandwidth up to 30 nm in the C-band with ± 0.5 dB uniformity (figures 8 and 9).

We stress that the design principles here illustrated are valid for any spatial mode and number N of waveguides. The ability to achieve different splitting ratios in the multi-input port configuration adds further flexibility to the device. Moreover, differently from Y-splitters and MMIs, arbitrary splitting ratio is achieved without increasing the system complexity. In this regard, it is worth noting that the fabrication of the proposed splitter would be based on standard and well-developed silicon platform and cleanroom nanofabrication techniques [32, 33]. Starting from a silicon-on-insulator wafer, the splitter would be patterned into silicon using e-beam lithography followed by a full reactive ion etching. Finally, a protective micron thick silica cladding would be deposited via plasma enhanced chemical vapor deposition.

It should also be noted that the ability to provide arbitrary power ratio does not come at the expenses of a large footprint or reduced bandwidth, which are comparable to recent solutions based on T-junctions and MMI technology [22, 23].

For all these reasons, we believe the proposed technology represents a viable solution to implement flexible and compact integrated power splitters for the multimode photonics platform.

Funding

This research is funded by the European Research Council under Grant Agreement No. 802 682 -ERC Starting Grant MODES.

Conflicts of interest

The authors declare no conflicts of interest.

Data availability statement

All data that support the findings of this study are included within the article (and any supplementary files).

Appendix. FEM simulations and mode decomposition

Differently from the coupled equations in equation (1), which implicitly assume the optical field to be carried by a single forward spatial mode, the FEM analysis accounts for the full spatial profile of light and allows analysing back-reflection, radiation losses and parasitic intermodal coupling that may arise due to bending, intermodal cross-talk and the discontinuity at the interface between the different stages.

In our simulations the system performance is simulated as a function of the wavelength λ. The total electric and magnetic fields in the waveguide W_n reads $\mathbf{E}(n,x,y,z)e^{i\omega t}$ and $\mathbf{H}(n,x,y,z)e^{i\omega t}$, with $\omega = 2\pi c/\lambda$. Since the transverse modes of each waveguide W_n represent a complete set of solutions for the Maxwell equations, $\mathbf{E}(n,x,y,z)$ and $\mathbf{H}(n,x,y,z)$ can be written as a linear combination of the forward and backward modes as follow [34]:

$$\mathbf{E}^{(t)}(n,x,y,z) = \sum_p [A_p(n,z) + B_p(n,z)]\mathbf{e}_p^{(t)}(n,x,y) \qquad (4a)$$

$$\mathbf{H}^{(t)}(n,x,y,z) = \sum_p [A_p(n,z) - B_p(n,z)]\mathbf{h}_p^{(t)}(n,x,y) \qquad (4b)$$

where $\mathbf{e}_p(n,x,y)$ and $\mathbf{h}_p(n,x,y)$ are respectively the electric and magnetic field of the p-spatial mode of waveguide W_n at wavelength λ, with superscript (t) indicating the transverse component (plane xy). $A_p(n,z)$ and $B_p(n,z)$ are respectively the forward and backward coefficients of the decomposition. For notational simplicity, here the summation $\sum$ includes the continuum of radiative (non-guided) modes.

The real part of the integral of the complex Poynting vector along z, namely $P_{tot}(n,z) = (1/2)\int_{xy} \Re[\mathbf{E}^{(t)}(n,x,y,z) \times \mathbf{H}^{*(t)}(n,x,y,z)]dxdy$, provides the total power flow at position z in the waveguide W_n [35]. We rewrite this integral by inserting the decomposition in equation (4), from which we find $P_{tot}(n,z) = \sum_p (|A_p(n,z)|^2 - |B_p(n,z)|^2)I_p(n)$, where $I_p(n) = (1/2)\int_{xy} \Re[\mathbf{e}_p^{(t)}(n,x,y) \times \mathbf{h}_p^{(*t)}(n,x,y)]dxdy$. Written in this way, we recognize the contribution to the total power of the forward (fwd) and backward (bwd) $p-$mode, namely, $P_{p,fwd}(n,z) = |A_p(n,z)|^2 I_p(n)$ and $P_{p,bwd}(n,z) = |B_p(n,z)|^2 I_p(n)$, respectively.

In the case of guided modes, the coefficients A_p and B_p can be easily isolated by exploiting the orthogonality relation between guided modes, i.e. $\int_{xy} \mathbf{e}_p^{(t)}(n,x,y) \times \mathbf{h}_q^{*(t)}(n,x,y)dxdy = 0$ if $q \neq p$. We multiply the left and right sides of equation (4a) by $\times \mathbf{h}_p^{*(t)}(n,x,y)$ and we integrate in xy. Similarly, we multiply the left and right sides of equation (4b) by $\times \mathbf{e}_p^{*(t)}(n,x,y)$ and we integrate in xy. Doing so, we finally find the following relations:

$$A_p = \frac{\int_{xy} \mathbf{E}_p^{(t)}(n,x,y) \times \mathbf{h}_p^{*(t)}(n,x,y)dxdy}{2I_p} + \frac{\int_{xy} \mathbf{H}_p^{(t)}(n,x,y) \times \mathbf{e}_p^{*(t)}(n,x,y)dxdy}{2I_p^*} \qquad (5a)$$

$$B_p = \frac{\int_{xy} \mathbf{E}_p^{(t)}(n,x,y) \times \mathbf{h}_p^{*(t)}(n,x,y)dxdy}{2I_p} - \frac{\int_{xy} \mathbf{H}_p^{(t)}(n,x,y) \times \mathbf{e}_p^{*(t)}(n,x,y)dxdy}{2I_p^*}. \qquad (5b)$$

These formulas describes the forward and backward power carried by each guided mode, and so ultimately allows evaluating reflection and radiation losses as well as the modal purity at the system output.

ORCID iD

Massimiliano Guasoni https://orcid.org/0000-0003-1526-5012

References

[1] Xue-Jian Z, Xue F, Deng-Ke Z and Yi-Dong H 2012 Compact temperature-insensitive modulator based on a silicon microring assistant Mach–Zehnder interferometer *Chin. Phys.* B **21** 124203

[2] Matsuo S, Yoshikuni Y, Segawa T, Ohiso Y and Okamoto H 2003 A widely tunable optical filter using ladder-type structure *IEEE Photonics Technol. Lett.* **15** 1114

[3] Novack A, Streshinsky M A, Ma Y and Hochberg M J, Variable power splitter for equalizing output power 2016 US Patent App. 14/963,205

[4] Desiatov B, Shams-Ansari A, Zhang M, Wang C and Lončar M 2019 Ultra-low-loss integrated visible photonics using thin-film lithium niobate *Optica* **6** 380

[5] Li Y, Li C, Li C, Cheng B and Xue C 2014a Compact two-mode (de)multiplexer based on symmetric Y-junction and multimode interference waveguides *Opt. Express* **22** 5781

[6] Tao S, Fang Q, Song J, Yu M, Lo G and Kwong D 2008 Cascade wide-angle Y-junction 1×16 optical power splitter based on silicon wire waveguides on silicon-on-insulator *Opt. Express* **16** 21456

[7] Zhang Y, Al-Mumin M, Liu H, Xu C, Zhang L, LiKawWa P L and Li G 2018 Integrated Power Splitters for Mode-Multiplexed Signals *Conference on Lasers and Electro-Optics (CLEO)* p JW2A–46

[8] Hosseini A, Kwong D N, Zhang Y, Subbaraman H, Xu X and Chen R T 2011 1 × N multimode interference beam splitter design techniques for on-chip optical interconnections *IEEE J. Sel. Top. Quantum Electron.* **17** 510

[9] Kwong D, Zhang Y, Hosseini A, Liu Y and Chen R T 2010 1 × 12 even fanout using multimode interference optical beam splitter on silicon nanomembrane *Electron. Lett.* **46** 1281

[10] Kawaguchi Y and Tsutsumi K 2002 Mode multiplexing and demultiplexing devices using multimode interference couplers *Electron. Lett.* **38** 1701

[11] May-Arrioja D, LiKamwa P, Velásquez-Ordóñez C and Sánchez-Mondragón J 2007 Tunable multimode interference coupler *Electron. Lett.* **43** 714

[12] Lin Z and Shi W 2019 Broadband, low-loss silicon photonic Y-junction with an arbitrary power splitting ratio *Opt. Express* **27** 14338

[13] Jiang W and Rahman B A 2018 Design of power-splitter with selectable splitting-ratio using angled and cascaded MMI-coupler *IEEE J. Quantum Electron.* **54** 1

[14] Wu X, Liu L, Zhang Y, Li D, Wang W and Xu L 2006 Low electric power drived thermo-optic multimode interference switches with tapered heating electrodes *Opt. Commun.* **258** 135

[15] Feng D J and Lay T 2008 Compact multimode interference couplers with arbitrary power splitting ratio *Opt. Express* **16** 7175

[16] Richardson D, Fini J and Nelson L E 2013 Space-division multiplexing in optical fibres *Nat. Photon.* **7** 354

[17] Li G, Bai N, Zhao N and Xia C 2014b Space-division multiplexing: the next frontier in optical communication *Adv. Opt. Photonics* **6** 413

[18] Krupa K, Tonello A, Shalaby B M, Fabert M, Barthélémy A, Millot G, Wabnitz S and Couderc V 2017 Spatial beam self-cleaning in multimode fibres *Nat. Photon.* **11** 237

[19] Lacava C *et al* 2019 Intermodal Bragg-scattering four wave mixing in silicon waveguides *J. Lightwave Technol.* **37** 1680

[20] Zhao Y *et al* 2020 Visible nonlinear photonics via high-order-mode dispersion engineering *Optica* **7** 135

[21] Carnio B and Elezzabi A 2020 Backward terahertz difference frequency generation via modal phase-matching in a planar LiNbO3 waveguide *Opt. Lett.* **45** 3657

[22] Zhang Y, Al-Mumin M A, Liu H, Xu C, Zhang L, LiKamWa P L and Li G 2019 An integrated few-mode power splitter based on multimode interference *J. Lightwave Technol.* **37** 3000

[23] Desai S, Yang G, Li L and Yi X 2020 Ultra-compact and low crosstalk 1 × N multimode interference splitter on silicon-on-insulator *14th Pacific Conf. on Lasers and Electro-Optics (CLEO PR 2020)* (Optical Society of America) p C11H3

[24] Badri S H and Gilarlue M M 2020 Multimode t-junctions based on truncated eaton lens *Frequenz* **74** 271

[25] Dai D, Wang J and Shi Y 2013 Silicon mode (de)multiplexer enabling high capacity photonic networks-on-chip with a single-wavelength-carrier light *Opt. Lett.* **38** 1422

[26] Sukhorukov A A and Kivshar Y S 2002 Discrete gap solitons in modulated waveguide arrays *Opt. Lett.* **27** 2112

[27] Yariv A and Yeh P 1984 *Optical Waves in Crystals* vol 5 (New York: Wiley)

[28] Li H 1980 Refractive index of silicon and germanium and its wavelength and temperature derivatives *J. Phys. Chem. Ref. Data* **9** 561

[29] Malitson I H 1965 Interspecimen comparison of the refractive index of fused silica *Josa* **55** 1205

[30] Thoms S, Macintyre D S, Docherty K E and Weaver J M 2014 Alignment verification for electron beam lithography *Microelectron. Eng.* **123** 9

[31] Boynton N, Pomerene A, Starbuck A, Lentine A and DeRose C T 2017 Characterization of systematic process variation in a silicon photonic platform *2017 IEEE Optical Conf. (OI)* (IEEE) pp 11–12

[32] Chen G F, Ong J R, Ang T Y, Lim S T, Png C E and Tan D T 2017 Broadband silicon-on-insulator directional couplers using a combination of straight and curved waveguide sections *Sci. Rep.* **7** 1

[33] Reed G T and Knights A P 2004 *Silicon Photonics: an Introduction* (New York: Wiley)

[34] Snyder A W and Love J 2012 *Optical Waveguide Theory* (US: Springer Science & Business Media)

[35] Someda C G 2017 *Electromagnetic Waves* (Boca Raton, FL: CRC Press)